Cell Host & Microbe, Volume *30*

Supplemental information

Lineage-mosaic and mutation-patched spike proteins for broad-spectrum COVID-19 vaccine

Yangtao Wu, Shaojuan Wang, Yali Zhang, Lunzhi Yuan, Qingbing Zheng, Min Wei, Yang Shi, Zikang Wang, Jian Ma, Kai Wang, Meifeng Nie, Jin Xiao, Zehong Huang, Peiwen Chen, Huilin Guo, Miaolin Lan, Jingjing Xu, Wangheng Hou, Yunda Hong, Dabing Chen, Hui Sun, Hualong Xiong, Ming Zhou, Che Liu, Wenjie Guo, Huiyu Guo, Jiahua Gao, Congling Gan, Zhixiong Li, Haitao Zhang, Xinrui Wang, Shaowei Li, Tong Cheng, Qinjian Zhao, Yixin Chen, Ting Wu, Tianying Zhang, Jun Zhang, Hua Cao, Huachen Zhu, Quan Yuan, Yi Guan, and Ningshao Xia

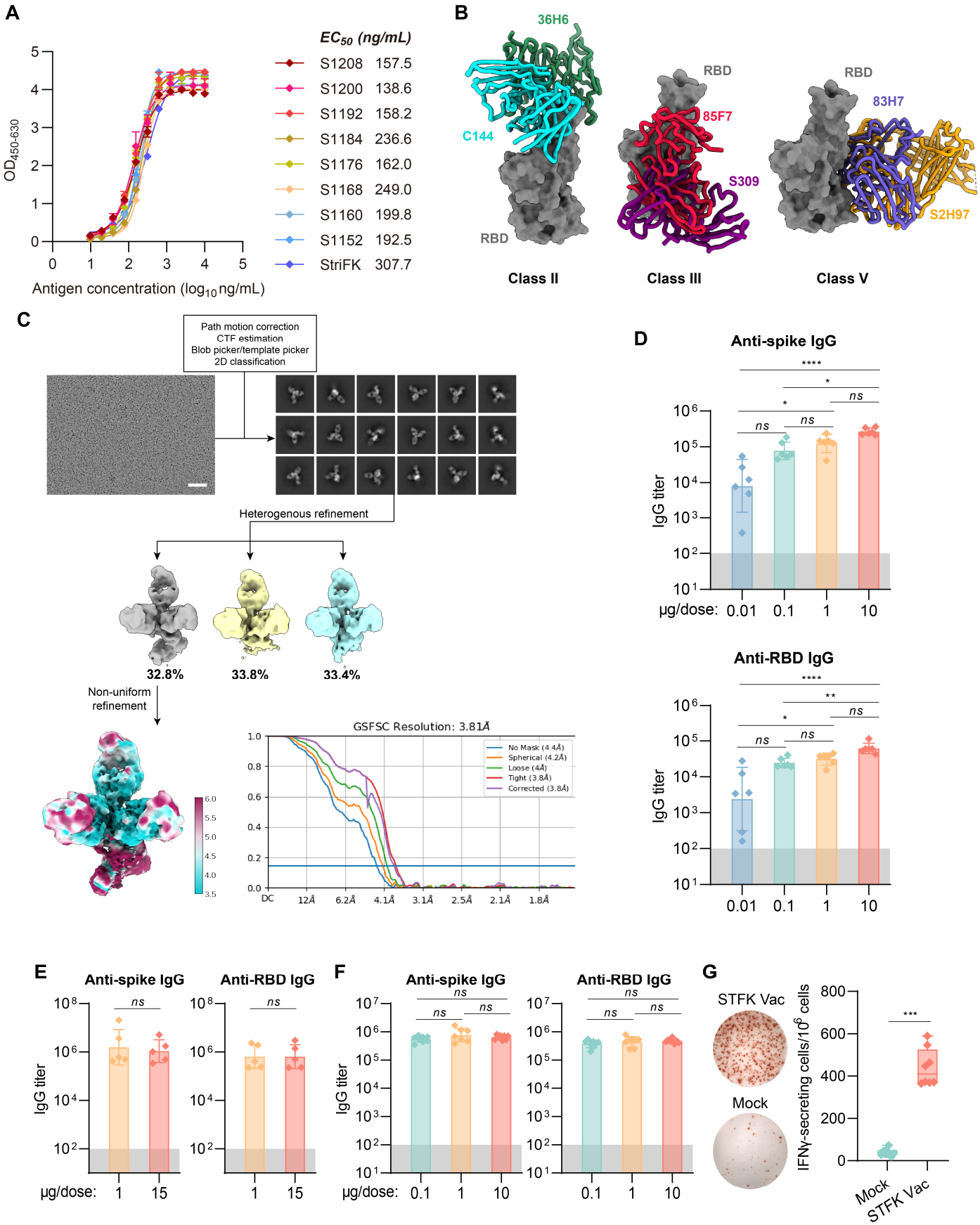

Figure S1. Evaluations for the recombinant STFK for *in vitro* binding with human rACE2 and *in vivo* immunogenicity. Related to Figure 1. (A) ELISA-binding activities of recombinant spike proteins with human rACE2. **(B)** 36H6, 85F7, and 83H7 were grouped into Class II, III, and V nAbs, and their binding modes are similar to reported nAbs C144 (Class II, pdb no. 7K90), S309 (Class III,

pdb no. 7R6W), and S2H97 (Class V, pdb no. 7M7W), respectively. **(C)** Flowchats of cryo-EM images processing and 3D reconstructions of STFK:36H6:83H7:85F7. Fourier shell correlation (FSC) curves and local resolution analysis of 3D and reconstructions are shown, scale bar=50 nm. **(D-F)** Anti-Spike and anti-RBD IgG titers in STFK-immunized BALB/c mice (D), rhesus monkeys (E), and hamsters (F). **(G)** Spike-specific T cell response elicited by STFK-vaccination in C57BL/6 mice measured by ELISpot assays. Representative images (right panel) and the counts of IFN-γ spot-forming cells (left panel) were shown. Data in (D-F) were plotted as the geometric mean with SD. Data in (G) were shown as box and whisker plots; median, first quartile, third quartile, minimum value, and maximum value were plotted. Dark shadows in (D-F) indicate the LOD. Uncorrected Kruskal-Wallis test (D, F) or Mann-Whitney *U* test (E, G) were used for intergroup statistical comparisons. Asterisks indicate statistical significance (****$P < 0.0001$; ***$P < 0.001$; **$P < 0.01$; *$P < 0.05$; ns, not significant).

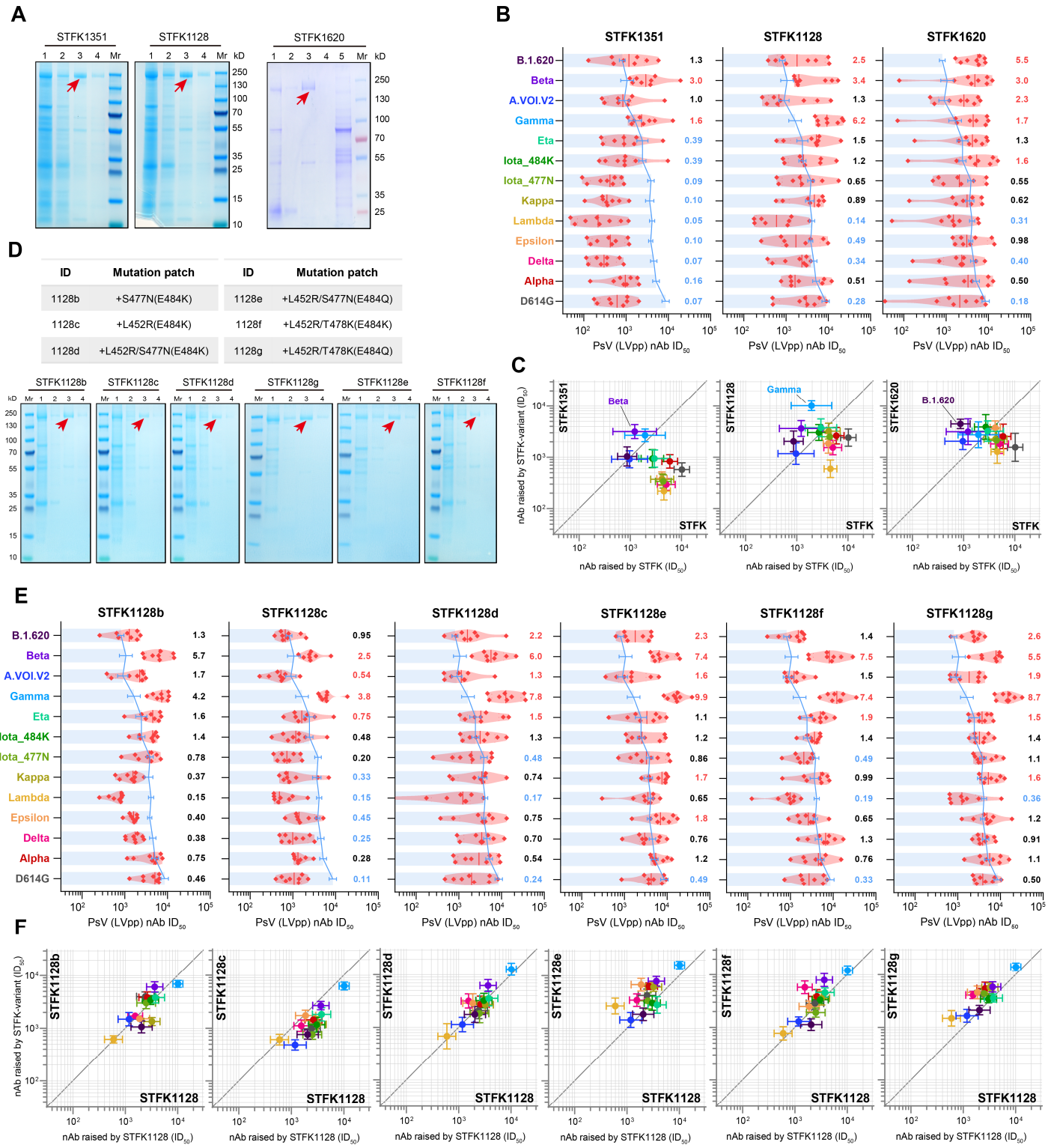

Figure S2. Neutralizing antibody responses elicited by STFK1351, STFK1128, STFK1620 and STFK1128 derivates in hamsters. Related to Figure 2. (A) SDS-PAGE analyses for STFK1351, STFK1128, and STFK1620. Mr, protein ladder; lane 1, supernatants of transfected cells; lane 2, flow-through fraction from the Q-FF column; lane 3-4, the eluate fractions with buffer containing 100 mM NaCl. The red arrow indicates the target protein band. **(B)** The nAb titers of sera from hamsters (n=8) receiving vaccination of STFK1351, STFK1128, and STFK1620 to neutralize lentiviral-pseudotyped SARS-CoV-2 variants. The blue lines (bars) indicate the nAb GMTs (±SD) induced by

the prototypic STFK vaccine against the corresponding variants. The numbers on the right represent the GMT fold-changes of nAb titers elicited by STFK variants to the prototypic STFK. The fold-changes were colored according to the values: <0.5 was in blue, 0.5-1.5 was in black, and >1.5 was in red. **(C)** The scatter plots compare the cross-neutralizing activities of nAbs raised by STFK variants (Y-axis) and prototypic STFK (X-axis). Data were plotted as the geometric mean with SEM. The diagonal line was Y=X. **(D)** Additional mutation patches in STFK1128 derivates compared to its parental construct and SDS-PAGE analyses for STFK1128 derivates. **(E)** The nAb titers of sera from hamsters (n=8) receiving vaccination of six STFK1128 derivates to neutralize lentiviral-pseudotyped SARS-CoV-2 variants. **(F)** The scatter plots show the comparison of nAbs against 13 variants raised by STFK1128 derivates (Y-axis) and their parental STFK1128 (X-axis).

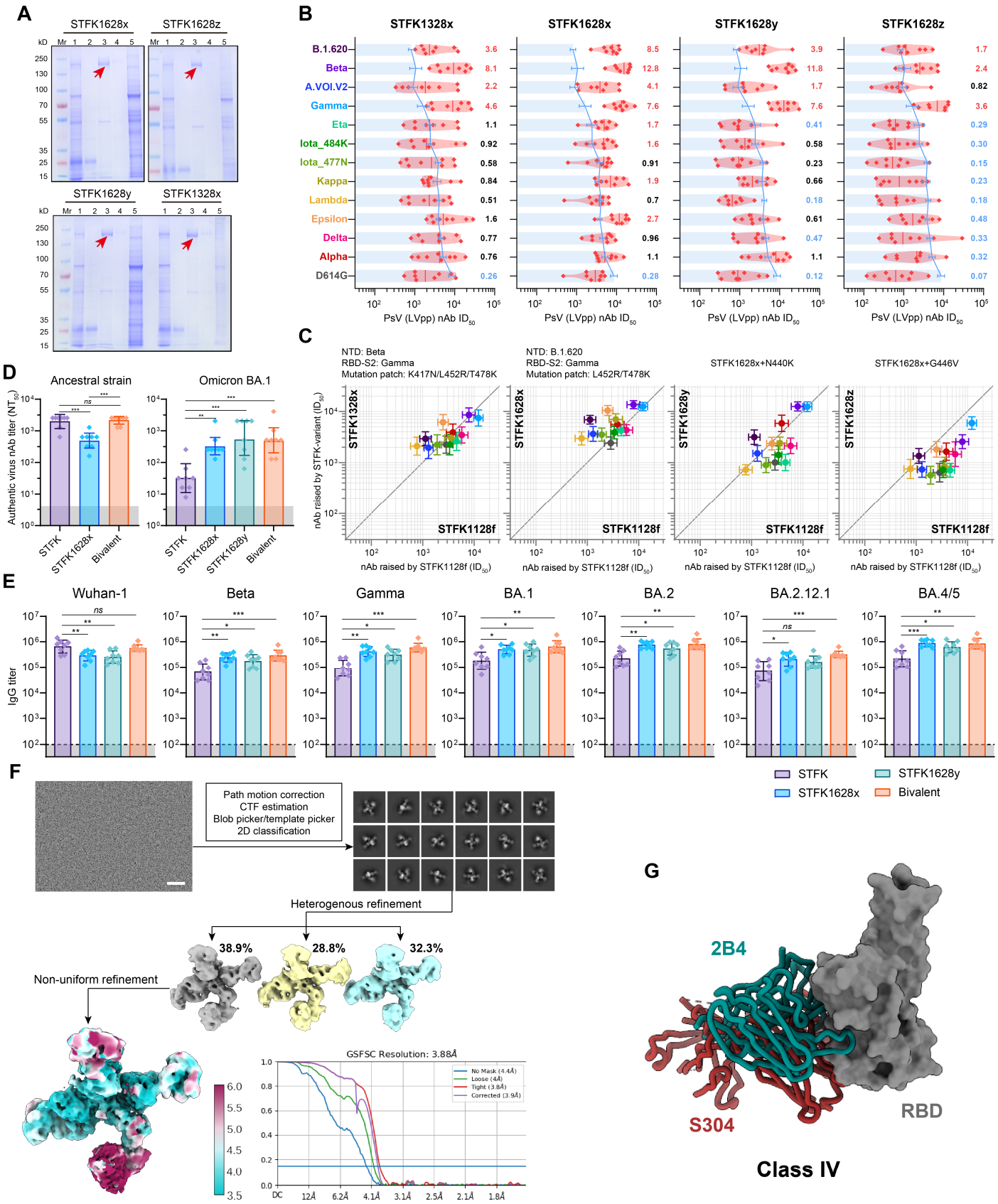

Figure S3. Neutralizing antibody responses elicited by inter-lineage chimeric STFK variants in hamsters. Related to Figure 2. (A) SDS-PAGE analyses for inter-lineage chimeric STFK variants. Mr, protein ladder; lane 1, supernatants of transfected cells; lane 2, flow-through fraction from the Q-FF column; lane 3-4, the eluate fractions with buffer containing 100 mM NaCl; lane 5,

eluate fraction with buffer containing 2 M NaCl. The red arrow indicates the target protein band. **(B)** The nAb titers of sera from hamsters (n=8) receiving vaccination of four STFK1128f-derived chimeric STFK variants to neutralize lentiviral-pseudotyped SARS-CoV-2 variants. The blue lines (bars) indicate the nAb GMTs (±SD) induced by the prototypic STFK vaccine against the corresponding variants. The numbers on the right represent the GMT fold-changes of nAb titers elicited by the chimeric STFK variants to the prototypic STFK. The fold-changes were colored according to the values: <0.5 was in blue, 0.5-1.5 was in black, and >1.5 was in red. **(C)** The scatter plots compare the cross-neutralizing activities of nAbs raised by chimeric STFK variants (Y-axis) and their parental STFK1128f (X-axis). Data were plotted as the geometric mean with SEM. The diagonal line was Y=X. A detailed information summary of each chimeric variant was shown on the top of the panels. **(D-E)** Serum authentic virus neutralizing antibodies (D) and anti-spike IgG responses against indicated spike proteins (E) elicited by engineered STFK variants in hamsters. Animals were identical to that shown in Figure 2. Data were plotted as GMT±SD. Dark shadows indicate the LOD. **(F)** Flowchats of cryo-EM images processing and 3D reconstructions of STFK1628x:83H7:85F7:2B4. Fourier shell correlation (FSC) curves and local resolution analysis of 3D and reconstructions are shown, scale bar=50 nm. **(G)** 2B4 was grouped into Class IV nAbs, and its binding mode is similar to reported nAbs S304 (Class IV, pdb no. 7R6X). Uncorrected Kruskal-Wallis test were used for intergroup statistical comparisons. Asterisks indicate statistical significance (***$P < 0.001$; **$P < 0.01$; ns, not significant).

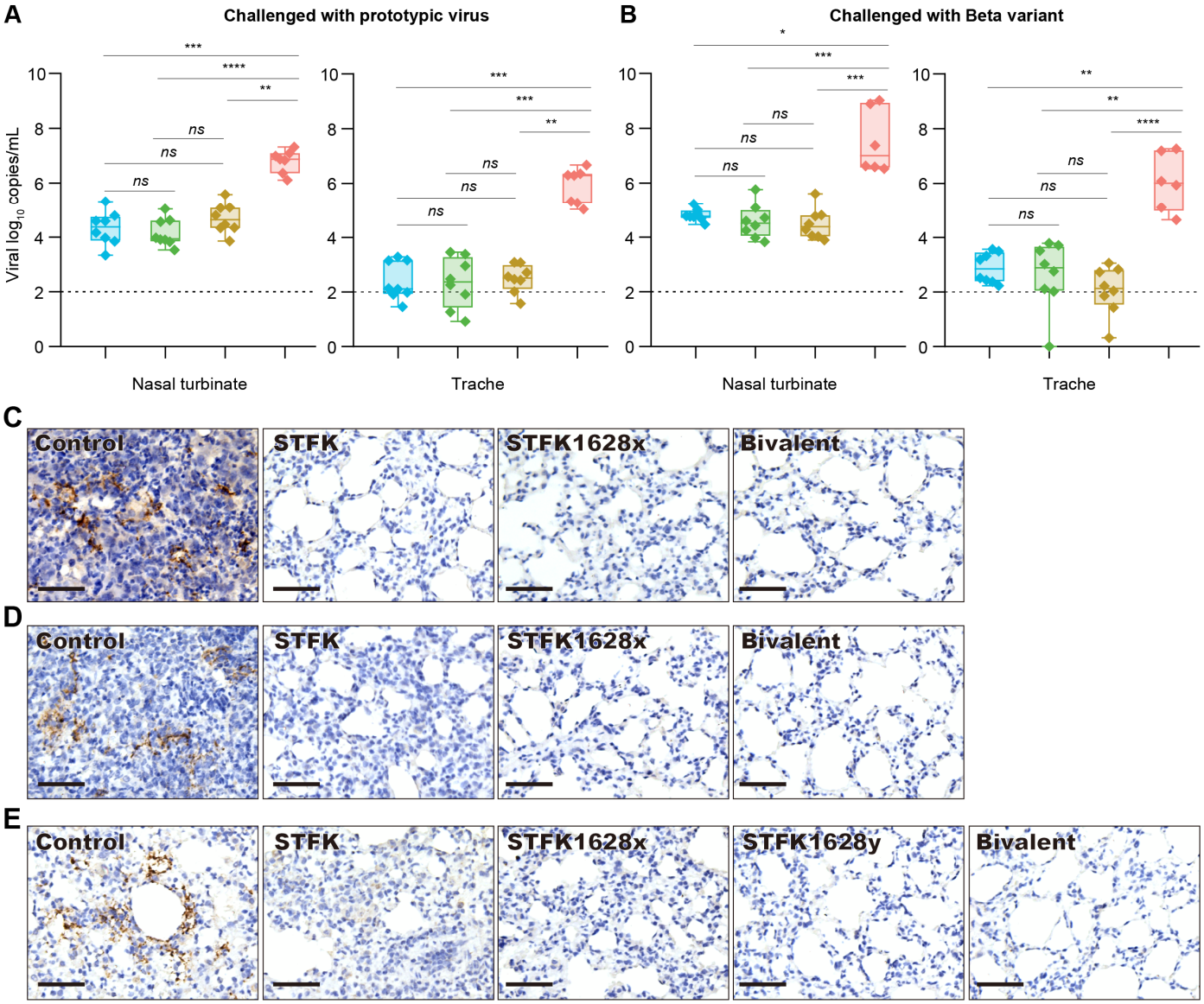

Figure S4 Tissue analyses for hamsters intranasally challenged with SARS-CoV-2. Related to Figure 3 and Figure 4. (A-B) Viral RNA levels in tissues of nasal turbinate (left panel) and trachea (right panel) collected from hamsters challenged with ancestral SARS-CoV-2 (A) or Beta variant (B). **(C-E)** Immunohistochemistry of SARS-CoV-2 N protein in hamster lungs. Representative lung sections from ancestral SARS-CoV-2 (C), Beta variant (D) or Omicron BA.1 (E) challenged hamsters. Scale bars indicate 50 μm. Uncorrected Kruskal-Wallis tests were used for intergroup statistical comparison. Asterisks indicate statistical significance (****P < 0.0001; ***P < 0.001; **P < 0.01; *P < 0.05; ns, not significant).

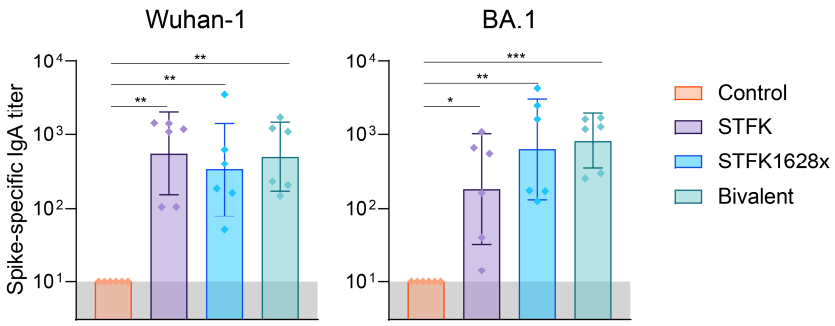

Figure S5. BAL anti-spike IgA response elicited by engineered STFK variants in mice. Related to Figure 5. BALB/c mice (n=6) were unvaccinated (Control) or vaccinated 2 dose (10 μg) of STFK, STFK1628x, or the bivalent at week 0 and 3. BAL fluid were collected two weeks after the booster, and were measured for Wuhan-1 strain or Omicron BA.1 spike-specific IgA by ELISA. Data were plotted as GMT±SD. Dark shadows indicate the LOD. Uncorrected Kruskal-Wallis tests were used for intergroup statistical comparisons. Asterisks indicate statistical significance (***$P < 0.001$; **$P < 0.01$; *$P < 0.05$).

Table S1. Cryo-EM data collection, refinement and validation statistics of three-antibody immune-complexes. Related to Figure 1 and Figure 2.

	STFK:36H6:83H7:85F7	STFK1628x:83H7:85F7:2B4
Data collection and processing		
Microscope	FEI TF30	FEI TF30
Camera	K3	K3
Magnification	39,000	39,000
Voltage (kV)	300	300
Electron exposure (e-/A2)	60	60
Defocus range (μm)	1.2-3.5	1.0-3.0
Pixel size (Å)	0.778	0.778
Micrographs (total)	3,479	4,191
Micrographs (used)	2,576	3,773
Total particle	1,146,590	1,684,307
Final particle images (no.)	162,177	115,589
Symmetry imposed	C1	C1
Map resolution (Å)	3.81	3.88
FSC threshold	0.143	0.143
Map sharpening B factor (Å2)	-142.4	-119.8
Validation		
MolProbity score	1.96	1.99
Clashscore	7.71	8.64
Poor rotamers (%)	0.69	0.00
RMS (bonds)	0.0113	0.0087
RMS (angles)	1.36	1.32
Ramachadran plot		
Favored (%)	90.44	90.91
Allowed (%)	9.44	8.97
Disallowed (%)	0.12	0.12